Journal of Nuclear Materials 389 (2009) 179–185

Contents lists available at ScienceDirect

Journal of Nuclear Materials

journal homepage: www.elsevier.com/locate/jnucmat

Thermal conductivity of $(U,Pu,Np)O_2$ solid solutions

Kyoichi Morimoto [a,*], Masato Kato [a], Masahiro Ogasawara [b], Motoaki Kashimura [a]

[a] Nuclear Fuel Cycle Engineering Laboratories, Japan Atomic Energy Agency, 4-33 Muramatsu, Tokai-mura, Naka-gun, Ibaraki 319-1194, Japan
[b] Inspection Development Company, 4-33 Muramatsu, Tokai-mura, Naka-gun, Ibaraki 319-1194, Japan

A B S T R A C T

The thermal conductivities of $(U,Pu,Np)O_2$ solid solutions were studied at temperatures from 900 to 1770 K. Thermal conductivities were obtained from the thermal diffusivity measured by the laser flash method. The thermal conductivities obtained below 1400 K were analyzed with the data of $(U,Pu,Am)O_2$ obtained previously, assuming that the B-value was constant, and could be expressed by a classical phonon transport model, $\lambda = (A + BT)^{-1}$, $A(z_1, z_2) = 3.583 \times 10^{-1} \times z_1 + 6.317 \times 10^{-2} \times z_2 + 1.595 \times 10^{-2}$ (m K/W) and $B = 2.493 \times 10^{-4}$ (m/W), where z_1 and z_2 are the contents of Am- and Np-oxides. It was found that the A-values increased linearly with increasing Np- and Am-oxide contents slightly, and the effect of Np-oxide content on A-values was smaller than that of Am-oxide content. The results obtained from the theoretical calculation based on the classical phonon transport model showed good agreement with the experimental results.

1. Introduction

Uranium-and-plutonium-mixed oxide (MOX) fuel has been so far used in fast breeder reactors (FBRs). Recently, the MOX fuel containing minor actinides (MAs) has become a candidate for a future nuclear fuel cycle, because it has high proliferation resistance and can reduce environmental burdens by decreasing the amount of MAs in high level radioactive waste [1,2]. In the development of MA-MOX fuel, thermal physical properties such as melting point and thermal conductivity are important for fuel design and performance analyses. When MAs are added to MOX fuel, these elements affect the thermal and mechanical properties of this fuel. Some studies have been reported on the effects of Np-oxide addition in UO_2 and MOX fuels on the thermal conductivity [3,4]. Also, evaluations of thermal conductivity of pure NpO_2 have been carried out [5,6]. There has, however, been no experimental study concerning the effect of Np-oxide addition into MOX fuel on the thermal conductivity of MOX fuel until now.

In the present study, the stoichiometric MOX fuels containing 6% and 12% of Np-oxide were prepared, and their thermal conductivities were measured. These results were compared with the thermal conductivities of MOX fuel containing Am-oxide previously obtained by Morimoto et al. [7].

2. Experimental

2.1. Preparation of specimens

The specimens in this study were MOX pellets containing two different amounts of Np (Np-MOX). One Np-MOX specimen containing about 6% Np of the total metal content and two Np-MOX specimens containing about 12% Np were prepared. Detailed compositions of these specimens are shown in Table 1. In this table, the content of Am generated by the decay of ^{241}Pu was taken into consideration.

The raw powders containing Np were prepared as follows. The Pu nitric acid solution obtained from the reprocessing plant of Japan Atomic Energy Agency (JAEA) contained about 1% Np. The Np concentration in this solution was enriched to an Np/Pu ratio of 0.5 by an anion exchange method. This solution was mixed with the plutonium nitrate and uranyl nitrate solutions to obtain $Np_{0.06}Pu_{0.30}U_{0.64}$ and $Np_{0.12}Pu_{0.30}U_{0.58}$ nitric acid solutions. These solutions were denitrated by microwave treatment and heated in an air and then reduced under an atmosphere of Ar–5% H_2 mixed gas to make powders. The main impurities of these powders are listed in Table 2. These powders were cold-pressed at 4.5 t/cm^2, and the compacts were sintered to pellets at about 1973 K for 3 h under an atmosphere of Ar–5% H_2 mixed gas. The oxygen-to-metal (O/M) ratios of specimens were adjusted to 2.00 by heating them at 1123 K for 5 h under an atmosphere of Ar–5% H_2 mixed gas containing a suitable amount of moisture. In the following sentences, the pellets of $(Np_{0.06}Pu_{0.30}U_{0.64})O_2$ and $(Np_{0.12}Pu_{0.30}U_{0.58})O_2$ are denoted as 6% Np-MOX and 12% Np-MOX, respectively.

After crushing a part of these stoichiometric specimens, the lattice parameters of the specimens were measured by an X-ray

* Corresponding author. Tel.: +81 29 282 1111; fax: +81 29 282 9473.
E-mail address: morimoto.kyoichi@jaea.go.jp (K. Morimoto).

0022-3115/$ - see front matter © 2009 Elsevier B.V. All rights reserved.
doi:10.1016/j.jnucmat.2009.01.026

Table 1
Main characteristic of the specimens.

Specimen (unit)	Np-01	Np-02	Np-03
Content (mol%)			
Np/(U + Pu + Am + Np)	5.90%	11.87%	11.87%
Pu/(U + Pu + Am + Np)	28.76%	28.97%	28.97%
Am/(U + Pu + Am + Np)	0.65%	0.85%	0.85%
Theoretical density (%TD)	93.0%	94.1%	94.1%
Diameter (mm)	5.219	5.569	5.684
Thickness (mm)	1.269	1.141	1.154
O/M ratio			
Before measurement	2.000	2.000	2.000
After measurement	–	1.999	–
Specimen weight (g)			
Before measurement	0.2827	0.2640	0.2610
After measurement	0.2820	0.2636	0.2606
Temperature range (K)	874–1780	1008–1793	992–1769

Table 2
Impurity analysis of the raw materials of 6% Np- and 12% Np-MOX.

Element	6% Np-MOX (ppm)	12% Np-MOX (ppm)
Ag	2	<2
Al	<50	<50
B	<2	<2
Ca	<50	<50
Cd	<2	<2
Cr	40	<20
Cu	3	<2
Fe	260	170
Mg	<20	<20
Mn	10	<10
Mo	<20	<20
Na	110	30
Ni	20	<20
Pb	<10	<10
Si	<20	<20
Sn	<20	<20
V	<50	<50
Zn	<50	<50

diffractometer (RINT-1100, Rigaku Co. Ltd.). As shown in Fig. 1, the lattice parameter analyzed from the diffraction patterns show good agreement with the parameters of these specimens calculated using Vegard's law [8]. In order to check the homogeneity of specimens, the element distribution of a transverse cross-section of two specimens was analyzed by an electron probe micro-analyzer (EPMA; JXA-8800, JOEL Ltd.). The EPMA mapping results of Fig. 2 shows that the specimens have a high degree of homogeneity.

2.2. Thermal diffusivity measurements and thermal conductivity calculation

The thermal conductivity $\lambda(T)$ was obtained by multiplying thermal diffusivity $\alpha(T)$, density $\rho(T)$ and heat capacity $C_p(T)$ according to the following equation:

$$\lambda(T) = \alpha(T)\rho(T)C_p(T). \quad (1)$$

The thermal diffusivities of stoichiometric specimens were measured at temperatures from 900 to 1770 K using a laser flash apparatus (TC-7000UVH, ULVAC-Riko Co. Ltd.). Details of this apparatus have been described elsewhere [7]. The data obtained experimentally were analyzed by the curve-fitting method [9], and thermal diffusivities were figured out. Measurements were repeated three times at each temperature, and thermal diffusivity was determined from the average of these data. As shown in Table 2, the changes of O/M ratio and specimen weight between before and after thermal diffusivity measurement were very slight. The densities of Np-MOX at room temperature were measured by the immersion method. The variation of density due to the thermal expansion during the measurement was taken into consideration by using the equation reviewed by Carbajo et al. [10]. The heat capacity of $(U,Pu,Np,Am)O_{2.00}$ was estimated by using Kopp's law

$$C_p[U_{0.7-z_1-z_2}, Pu_{0.3}, Am_{z_1}, Np_{z_2}O_2] = (0.7 - z_1 - z_2) \times C_p(UO_2) + C_p(PuO_2) + z_1 \times C_p(AmO_2) + z_2 \times C_p(NpO_2), \quad (2)$$

where $C_p(UO_2)$ [10], $C_p(PuO_2)$ [10], $C_p(AmO_2)$ [11] and $C_p(NpO_2)$ [12] are the heat capacities of UO_2, PuO_2, NpO_2 and AmO_2, respectively.

The porosity influences of specimens on thermal conductivities were corrected by the modified Maxwell–Eucken relation: $F(p) = (1 - p)/(1 - \beta p)$, where $\beta = 0.5$ was from the result of Morimoto et al. [7]. The thermal conductivities λ_0 of a 100% theoretical density specimen were obtained from the conductivity λ of a real specimen at porosity p.

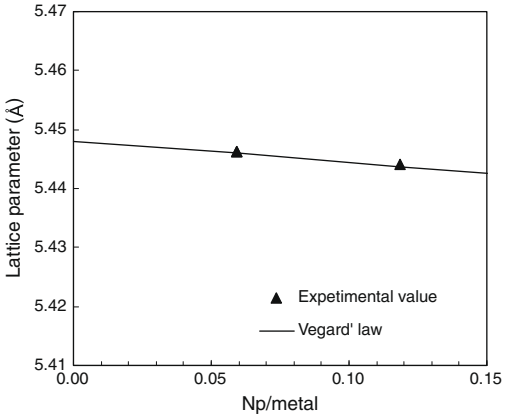

Fig. 1. Lattice parameters of near-stoichiometric 6% Np-MOX and 12% Np-MOX as a function of the Np ratio of the total metal content. The lattice parameter of $(U_{0.7-z1-z2}Pu_{0.3}Am_{z1}Np_{z2})O_2$ is calculated from Vegard's law.

3. Results and discussion

3.1. Experimental results

The thermal conductivities of Np-MOX specimens are shown in Fig. 3 as a function of temperature together with conductivities of MOX fuel containing Am (Am-MOX) investigated previously [7]. Although the effects of additions of Np-oxide and Am-oxide on thermal conductivity of MOX are not so large, the effect of addition of Np-oxide is smaller than that of Am-oxide. That is, the thermal conductivities of 6% Np-MOX are larger than those of 3% Am-MOX, which are nearly the same as to the thermal conductivities of 12% Np-MOX. The reason for this can be explained as follows. The difference of ionic radii between U and Np is smaller than that one between U and Am, and then the distortion, which is introduced by adding the MA and contributes to phonon scattering, is smaller in Np-MOX than in Am-MOX.

The dependence of Np ratio of the total metal content (Np-content) on thermal conductivities at 1073, 1273 and 1473 K is shown in Fig. 4. The thermal conductivities decrease slightly with an increase of Np-content.

Comparisons of the temperature dependences of thermal conductivities of UO_2, NpO_2, $(U,Np)O_2$ and Np-MOX are shown in Fig. 5. Experimental results are for UO_2 and Np-MOX observed by Morimoto et al. [7], for NpO_2 by Nishi et al. [5], for $(U,Np)O_2$ by Schmidt et al. [3] and for UO_2 by Hirai [13]. The data for Np-MOX by Katayama et al. [4] were theoretically obtained by using

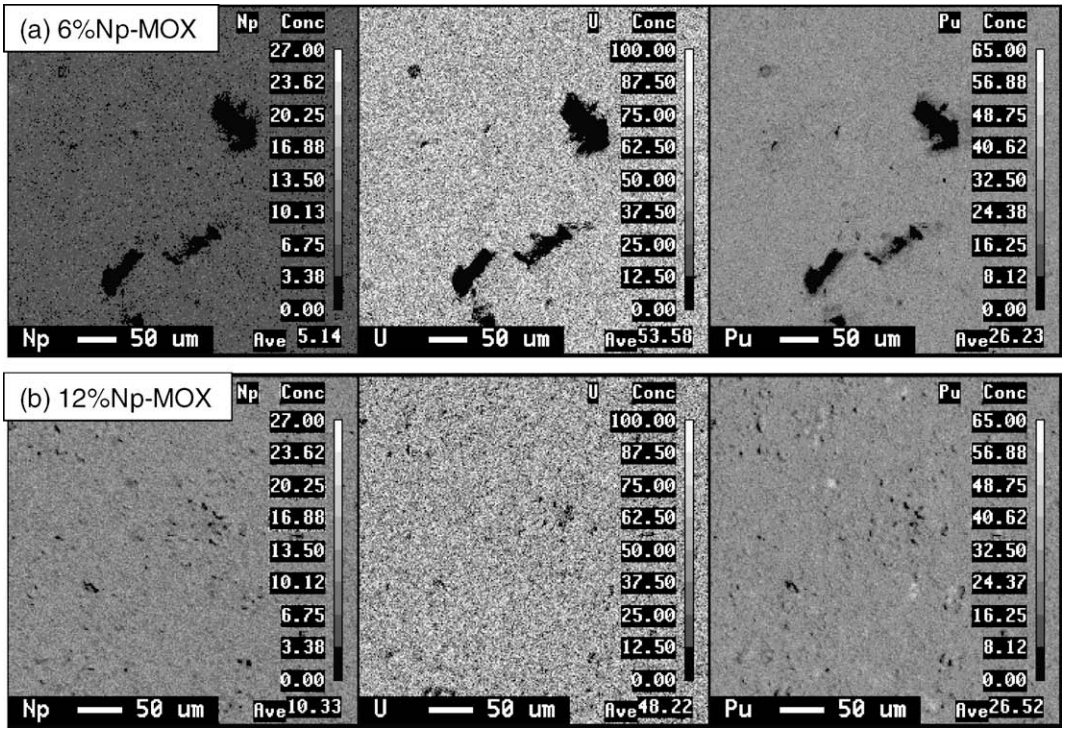

Fig. 2. EPMA mapping results of the cross-section of specimens: (a) results of 6% Np-MOX; (b) results of 12% Np-MOX.

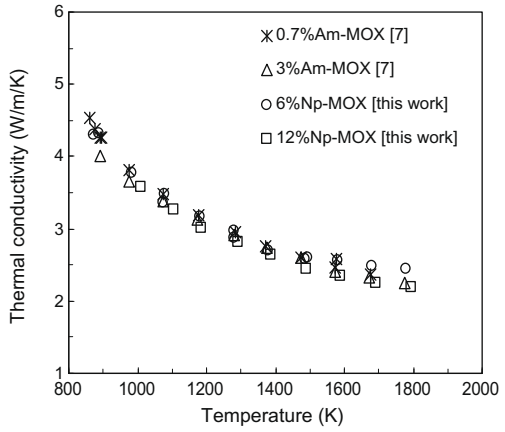

Fig. 3. Comparison of thermal conductivities of near-stoichiometric Np-MOX and near-stoichiometric Am-MOX.

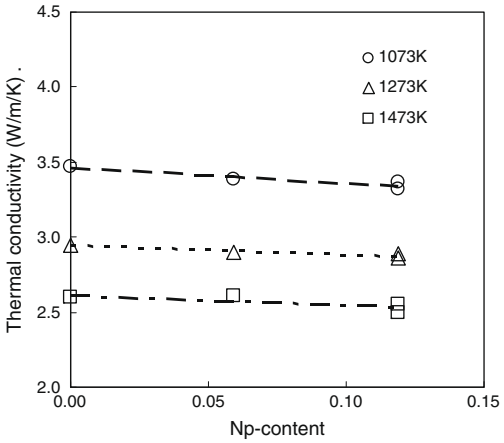

Fig. 4. Thermal conductivities of near-stoichiometric specimens as a function of Np-oxide content.

molecular dynamics calculations. The data for UO_2 by Hirai were estimated by multiplying thermal diffusivities and densities measured by Hirai himself and heat capacities estimated by the present authors. From these results, it is found that the temperature dependence of thermal conductivities of UO_2, NpO_2, $(U,Np)O_2$ and Np-MOX are very similar to each other.

The thermal resistivities, the reciprocals of thermal conductivities, of all specimens increase linearly with temperature up to about 1400 K. So, the thermal conductivities of Np-MOX can be expressed in the temperature region below 1400 K by the following equation based on a classical phonon transport model of dielectric solids above their Debye temperature:

$$\lambda = (A + BT)^{-1}. \quad (3)$$

The constant A in Eq. (3) is the lattice defect thermal resistivity due to the interaction of phonons with the lattice defect, and BT corresponds to the intrinsic lattice thermal resistivity due to the phonon–phonon interactions based on the Umklapp process. The values of A and B in the thermal conductivity of Np-MOX were determined by fitting the experimental data to Eq. (3). Here the slight content of Am-oxide generated by the decay of ^{241}Pu was taken into consideration. It was found from several fittings of experimental data to above equation, that slight changes of the B-value affected greatly the derivation of the A-value. If the B-value is changed, good data on the dependence of A-value on the content of Np cannot be obtained.

In the previous study on the thermal conductivities of Am-MOX [7], B-value was nearly constant, independent of the Am ratio of total metal (Am-content). Also in the study of Fukushima et al. [14] on the thermal conductivities of MOX containing rare earth oxides, the effect of rare earth oxide addition on the thermal conductivities was mainly caused by the lattice defects related to the A-value, and

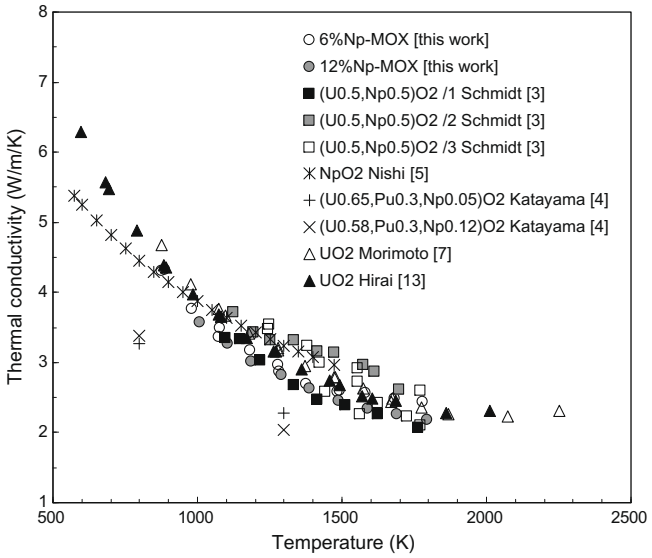

Fig. 5. Comparison of thermal dependences of thermal conductivities of oxides containing Np [3,4,5] and of UO_2 [7,13]. The thermal conductivities of $(U_{0.5},Np_{0.5})O_2$, NpO_2 and UO_2 are experimental values. Those of $(U_{0.65},Pu_{0.3},Np_{0.05})O_2$ and $(U_{0.58},Pu_{0.3},Np_{0.12})O_2$ are obtained by using molecular dynamics calculations.

the *B*-value was constant independent of rare earth oxide contents. Then, *B*-value was assumed to be constant, and the results obtained previously and in this study (Fig. 3) were fitted to Eq. (3). From this, the *A*- and *B*-values were expressed as a function of Am and Np-oxides contents by the following equations:

$$A = 3.583 \times 10^{-1} \times z_1 + 6.317 \times 10^{-2} \times z_2 + 1.595 \times 10^{-2} (mK/W),$$

$$B = 2.493 \times 10^{-4} (m/W),$$

where z_1 and z_2 are Am-content and Np-content, respectively. Here, the results obtained in the previous study were re-evaluated by lowering the highest temperature from 1500 to 1400 K.

Table 3 shows *A*-values obtained from fitting results of experimental data. Fig. 6 shows the dependence of *A*-values on Am- and Np-contents. *A*-values of thermal conductivities of Np-MOX and Am-MOX decrease with increasing contents of Np- and Am-oxide, respectively, but their increase rate is larger in Am-MOX than in Np-MOX. This reason can be also understood from the difference of ionic radii between U–Np and U–Am in MOX, as already described.

3.2. Lattice defect thermal resistivity

According to a classical phonon transport model of dielectric solids above their Debye temperature, the *A*-value in Eq. (3) is the lattice defect thermal resistivity, due to the interaction of phonons with the lattice defect. BT corresponds to the intrinsic lattice thermal resistivity due to the phonon–phonon interactions based on the Umklapp process.

Table 3
Fitting results of coefficient *A* (coefficient *B* was fixed at 2.493×10^{-4}).

Specimen	Am-content (%)	Np-content (%)	*A*-value
0.7% Am-MOX	0.68	0.00	1.827×10^{-2}
2% Am-MOX	2.20	0.00	2.279×10^{-2}
3% Am-MOX	3.09	0.00	2.750×10^{-2}
6% Np-MOX	0.65	5.90	2.237×10^{-2}
12% Np-MOX	0.85	11.87	2.685×10^{-2}

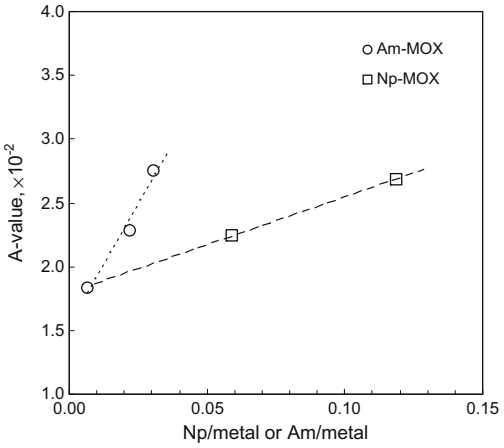

Fig. 6. Comparison of *A*-values in thermal conductivity of Np-MOX and of Am-MOX. Symbols are *A*-values obtained from the experimental data. The dashed lines show the results determined by a linear regression of the *A*-values.

Ambegaoker [15] obtained the following relationship for the lattice defect thermal resistivity, *A*, by using Klemen's theory [16]

$$A = \frac{\pi^2 \overline{V} \theta}{3 \overline{v}^2 h} \sum_i \Gamma_i = C \sum_i \Gamma_i, \tag{4}$$

where $\overline{V} = a^3/12$, is the average atomic volume obtained from lattice parameter a, θ the Debye temperature, $\overline{v}$ the average phonon velocity, and *h* Planck's constant. Γ_i is a scattering cross-section parameter of phonons by point defect *i* and is approximately given by the following equation [17]:

$$\Gamma_i = X_i \left[\left(\frac{\overline{M} - M_i}{\overline{M}} \right)^2 + \varepsilon \left(\frac{\overline{r} - r_i}{\overline{r}} \right)^2 \right], \tag{5}$$

where X_i and M_i are the atomic fraction and the mass of point defect *i*, respectively. $\overline{M}$ is the average atomic mass of the host lattice site, r_i the atomic radius of the point defect *i* in its own lattice, and $\overline{r}$ the average atomic radius of the host lattice site. The parameter ε is one which represents the magnitude of lattice strain generated by the point defect and is obtained by fitting the experimental data to Eq. (5).

The sum of Γ_i is expressed as

$$\sum_i \Gamma_i = \left(\frac{\sum_i X_i M_i^2 - \overline{M}^2}{\overline{M}^2} \right) + \varepsilon \left(\frac{\sum_i X_i r_i^2 - \overline{r}^2}{\overline{r}^2} \right). \tag{6}$$

In this study, the contents of Np in the specimens were about 6% and 12%. It is known in actinide compounds that U can exist as U^{4+}, U^{5+} and U^{6+}, Pu as Pu^{3+} and Pu^{4+}, Am as Am^{3+} and Am^{4+}, and Np as Np^{4+}. Thus, a lot of combinations of different cation valences can be considered in these compounds. From the results of Morimoto et al. [7], it was assumed that the combination of U^{4+}, U^{5+}, Pu^{4+} and Am^{3+} is suitable in the stoichiometric $(U,Pu,Am)O_2$. In the case of Np-oxide, Richter and Gerontopoulos [18] indicated that Np^{4+} could not be reduced and oxidized. It was assumed from these results that the ionic structures, $(U^{4+},Pu^{4+})O_2$, $(U^{4+},U^{5+},Pu^{4+},Am^{3+})O_2$, $(U^{4+},U^{5+},Pu^{4+},Am^{3+},Np^{4+})O_2$ could be applied to the MOX, Am-MOX and Np-MOX. In addition, only cations in the cation sublattice were taken consideration because the amount of O^{2-} ion is independent of changes of cations in the stoichiometric compounds.

Also in this study, the evaluations of *A*- and *B*-values were carried out, using the same method as in previous studies [7,14].

Table 4
Constants used in the phonon scattering model calculation of *A*- and *B*-values.

Constant (unit)	Nomenclature	Numerical value
Mass number		
UO_2	M_{UO_2}	270
NpO_2	M_{NpO_2}	269
PuO_2	M_{PuO_2}	271
AmO_2	M_{AmO_2}	273
Lattice parameter (nm)		
UO_2	a_{UO_2}	0.54702
NpO_2	a_{NpO_2}	0.54339
PuO_2	a_{PuO_2}	0.53960
AmO_2	a_{AmO_2}	0.53772
Debye temperature of UO_2 (K)	θUO_2	242
Average phonon velocity in UO_2 (m/s)	V_{UO_2}	4300
Melting point (K)		
UO_2	TM_{UO_2}	3123
NpO_2	TM_{NpO_2}	2820
PuO_2	TM_{PuO_2}	2843
AmO_2	TM_{AmO_2}	2773
Heat of fusion (kJ/mol)		
UO_2	HF_{UO_2}	77.9
NpO_2	HF_{NpO_2}	70.6
PuO_2	HF_{PuO_2}	70.9
AmO_2	HF_{AmO_2}	69.1

Generally, the lattice defect thermal resistivity A can be expressed as follows:

$$A = W_1 = W_1(0) + \Delta W_1(x), \tag{7}$$

where $W_i(0)$ is the lattice defect thermal resistivity caused by impurities, grain boundary and so on. $\Delta W_i(x)$ is the other lattice defect thermal resistivity caused by adding the MAs oxides. In the following expression, A-values in the thermal conductivities of MOX, Am-MOX and Np-MOX are described as A_{MOX}, $A_{Am\text{-}MOX}$ and $A_{Np\text{-}MOX}$, respectively.

$A_{Am\text{-}MOX}$ was compared with A_{MOX} in order to evaluate the effect of Am-oxide content (ΔA_{Am}), and $A_{Np\text{-}MOX}$ was compared with $A_{Am\text{-}MOX}$ in order to evaluate the effect of Np-oxide content (ΔA_{Np}). That is, the following two differences of A-values were analyzed

$$\Delta A_{Am} = \Delta W_{1\text{-}Am}(x) = A_{Am-MOX} - A_{MOX} = C_{Am-MOX}\sum_j \Gamma_j - C_{MOX}\sum_i \Gamma_i, \tag{8}$$

$$\Delta A_{Np} = \Delta W_{1\text{-}Np}(x) = A_{Np-MOX} - A_{Am-MOX} = C_{Np-MOX}\sum_j \Gamma_j - C_{Am-MOX}\sum_i \Gamma_i. \tag{9}$$

The details of coefficient C in Eqs. (8) and (9) are shown in Eq. (4). The Debye temperature and the average phonon velocity of MA-MOX which is necessary to obtain C were calculated by the following equations:

$$\theta_{MA-MOX} = \theta_{UO_2}\frac{(\overline{M}_{UO_2})^{1/2}(\overline{V}_{UO_2})^{1/3}(TM_{MA-MOX})^{1/2}}{(\overline{M}_{MA-MOX})^{1/2}(\overline{V}_{MA-MOX})^{1/3}(TM_{UO_2})^{1/2}}, \tag{10}$$

$$\overline{v}_{MA-MOX} = \overline{v}_{UO_2}\left(\frac{\theta_{MA-MOX}}{\theta_{UO_2}}\right)\left(\frac{a_{MA-MOX}}{a_{UO_2}}\right), \tag{11}$$

where TM_{UO_2} and $TM_{MA\text{-}MOX}$ are melting points of UO_2 and MA-MOX, a_{UO_2} and a_{MA-MOX} are lattice parameters, $\overline{M}_{UO_2}$ and $\overline{M}_{MA-MOX}$ are the average atomic masses, and $\overline{V}_{UO_2}$ and $\overline{V}_{MA-MOX}$ are the average atomic volumes. The melting points of MA-MOX were calculated from the melting point and the heat of fusion of all components in MA-MOX (UO_2, PuO_2, AmO_2 and NpO_2) by using the ideal solution model [19]. The lattice parameters of MA-MOX were estimated from the lattice parameters of these components by using Vegard's law [8]. The data for calculation of coefficient C are listed in Table 4.

Table 5
Ionic radii used in this study.

Ion		Radius (nm)
Anion	CN = 4	
O^{2-}		0.1380 [20]
Cation	CN = 8	
U^{4+}		0.1000 [20]
U^{5+}		0.0880 [21]
Np^{4+}		0.0980 [20]
Pu^{3+}		0.1100 [21]
Pu^{4+}		0.0960 [20]
Am^{3+}		0.1090 [20]
Am^{4+}		0.0950 [20]

In the analysis using the phonon scattering model, it is impossible to evaluate the effects of Np- and Am-oxide contents on A-value if both contents are changed simultaneously. Accordingly, the effects of Np- and Am-oxide content on thermal conductivity were evaluated individually.

The lattice defect thermal resistivity of Am-MOX, $A_{Am\text{-}MOX}$, is described as follows:

$$A_{Am-MOX} = C_{Am-MOX}\sum_i \Gamma_j = C_{Am-MOX}\left[\left\{\frac{(X_{U^{4+}}+X_{U^{5+}})M_U^2 + X_{Pu^{4+}}M_{Pu}^2 + X_{Am^{3+}}M_{Am}^2}{\overline{M}_{Am-MOX}^2} - 1\right\} + \varepsilon\left\{\frac{X_{U^{4+}}r_{U^{4+}}^2 + X_{U^{5+}}r_{U^{5+}}^2 + X_{Pu^{4+}}r_{Pu^{4+}}^2 + X_{Am^{3+}}r_{Am^{3+}}^2}{\overline{r}_{Am-MOX}^2} - 1\right\}\right], \tag{12}$$

where $\overline{M}_{Am-MOX}$ is the average atomic mass of the elements contained in Eq. (12) and $\overline{r}_{Am-MOX} = (0.7-2z_1)r_U^{4+} + z_1 r_U^{5+} + 0.3r_{Pu}^{4+} + z_1 r_{Am}^{3+}$. The cation and anion radii are shown in Table 5.

The lattice defect thermal resistivity of MOX, A_{MOX}, is described as follows:

$$A_{MOX} = C_{MOX}\sum_i \Gamma_j = C_{MOX}\left[\left\{\frac{X_{U^{4+}}M_U^2 + X_{Pu^{4+}}M_{Pu}^2}{\overline{M}_{MOX}^2} - 1\right\} + \varepsilon\left\{\frac{X_{U^{4+}}r_{U^{4+}}^2 + X_{Pu^{4+}}r_{Pu^{4+}}^2}{\overline{r}_{MOX}^2} - 1\right\}\right], \tag{13}$$

where $\overline{M}_{MOX}$ is the average atomic mass of the elements contained in Eq. (13) and $\overline{r}_{MOX} = 0.7r_U^{4+} + 0.3r_{Pu}^{4+}$.

In the case of Np-MOX, a small amount of Am has to be taken into account because ^{241}Am accumulates gradually by the decay of ^{241}Pu. The lattice defect thermal resistivity of Np-MOX, $A_{Np\text{-}MOX}$, is described as follows:

$$A_{Np-MOX} = C_{Np-MOX}\sum_i \Gamma_j = C_{Np-MOX}\left[\left\{\frac{(X_{U^{4+}}+X_{U^{5+}})M_U^2 + X_{Pu^{4+}}M_{Pu}^2 + X_{Am^{3+}}M_{Am}^2 + X_{Np^{4+}}M_{Np}^2}{\overline{M}_{Np-MOX}^2} - 1\right\} + \varepsilon\left\{\frac{X_{U^{4+}}r_{U^{4+}}^2 + X_{U^{5+}}r_{U^{5+}}^2 + X_{Pu^{4+}}r_{Pu^{4+}}^2 + X_{Am^{3+}}r_{Am^{3+}}^2 + X_{Np^{4+}}r_{Np^{4+}}^2}{\overline{r}_{Np-MOX}^2} - 1\right\}\right], \tag{14}$$

where $\overline{M}_{Np-MOX}$ is the average atomic mass of the elements contained in Eq. (14) and $\overline{r}_{Np-MOX} = (0.7-2z_1-z_2)r_U^{4+} + z_1 r_U^{5+} + 0.3r_{Pu}^{4+} + z_1 r_{Am}^{3+} + z_2 r_{Np}^{4+}$.

The two dependencies of Np- and Am-oxide contents on A-values were theoretically calculated by using Eqs. (4)–(14). Fig. 7 shows the obtained dependences of A-values on Am- and

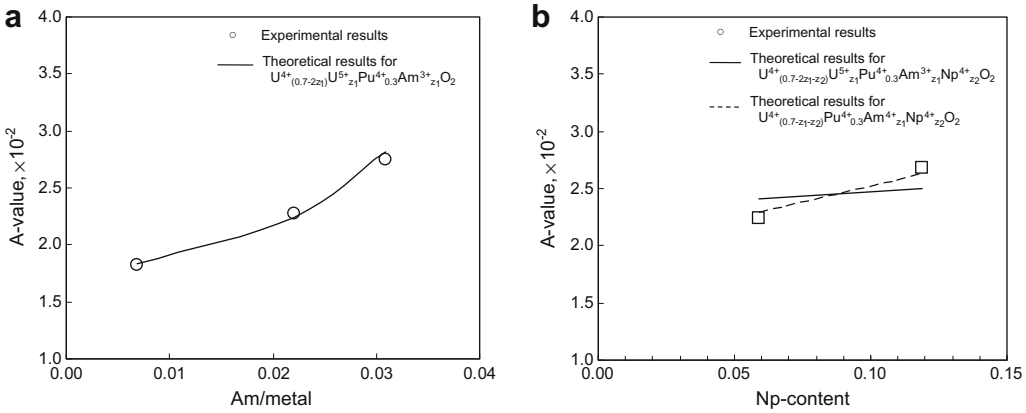

Fig. 7. Comparison between the experimental and theoretical *A*-values. (a) Experimental results for Am-MOX. Theoretical results for $(U^{4+},U^{5+},Pu^{4+},Am^{3+})O_2$. (b) Experimental results for Np-MOX. Theoretical results for $(U^{4+},U^{5+},Pu^{4+},Am^{3+},Np^{4+})O_2$ and $(U^{4+},Pu^{4+},Am^{4+},Np^{4+})O_2$.

Np-oxides contents for the thermal conductivities of Am-MOX and Np-MOX, assuming that ε-values were 32 for Am-MOX and 45 for Np-MOX, respectively. In the case of Am-MOX, the agreement between experimental and theoretical results is fairly good, but is not so good in the case of Np-MOX.

As a trial to improve the agreement in the case of Np-MOX, *A*-value was calculated in another ionic composition, $(U^{4+},Pu^{4+},Am^{4+},Np^{4+})O_2$. These results are also shown also in Fig. 7(b). A good agreement can be seen between both experimental and theoretical dependences. Although the reason for this cannot be fully understood, it is suggested that the addition of Np-oxide prevents the conversion of U^{4+} to U^{5+}, resulting in the prevent of Am^{4+} to Am^{3+} because the contents of Am in Np-MOX are so small.

3.3. Intrinsic lattice thermal resistivity

In the studies on thermal conductivity of oxide fuels, many authors [14,22–25] have used the following Liebfried–Schlömann relationship to explain the intrinsic lattice thermal resistivity

$$\mathrm{BT} = \frac{\gamma^2 T}{\left[\frac{24}{10}4^{1/3}\left(\frac{h}{k}\right)^3 \overline{M}\cdot\overline{V}^{1/3}\theta^3\right]}, \tag{15}$$

where γ is the Grüneisen constant, h Planck's constant, k the Boltzmann constant, $\overline{M}$ the average atomic mass of the host lattice site, $\overline{V}$ the average atomic volume, and θ the Debye temperature.

It has been reported by Gibby [22] and Duriez et al. [23] that the *B*-values predicted by using Eq. (15) were 3 or 4 times lower than experimental values. As shown in both these studies, the relative ratio of B_1-value for compound 1 to B_2-value for compound 2 could be expressed by the following equation, based on the Lindeman relationship which express θ as a function of the melting point [22]

$$\frac{B_2}{B_1} = \left(\frac{M_2}{M_1}\right)^{1/2}\left(\frac{a_2}{a_1}\right)^2\left(\frac{\mathrm{TM}_1}{\mathrm{TM}_2}\right)^{3/2}\left(\frac{\gamma_2}{\gamma_1}\right)^2, \tag{16}$$

where M_i, a_i, TM_i and γ_i are the molecular weight, the lattice parameter, the melting point and the Grüneisen constant for compound i, respectively.

In the evaluation of *B*-values of Np-MOX and Am-MOX, compounds 1 and 2 of Eq. (16) were assumed as UO_2 and MA-MOX, respectively, as shown in Eq. (17)

$$\frac{B_{\mathrm{MA-MOX}}}{B_{\mathrm{UO_2}}} = \left(\frac{M_{\mathrm{MA-MOX}}}{M_{\mathrm{UO_2}}}\right)^{1/2}\left(\frac{a_{\mathrm{MA-MOX}}}{a_{\mathrm{UO_2}}}\right)^2\left(\frac{T_{\mathrm{UO_2}}}{T_{\mathrm{MA-MOX}}}\right)^{3/2}\left(\frac{\gamma_{\mathrm{MA-MOX}}}{\gamma_{\mathrm{UO_2}}}\right)^2. \tag{17}$$

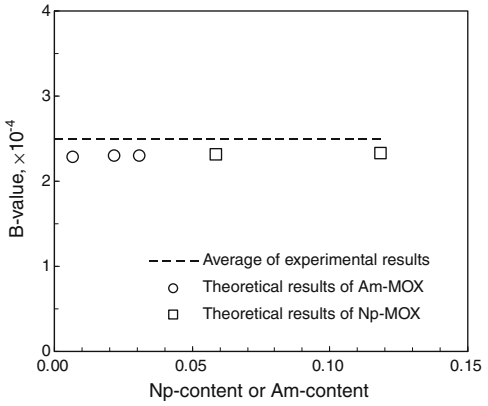

Fig. 8. Comparison between the experimental and theoretical *B*-values.

As described by Gibby [22] and Duriez et al. [23], it was assumed that the Grüneisen constants of Np-MOX and Am-MOX were same as that of UO_2 and $\gamma_{\mathrm{MA\text{-}MOX}}/\gamma_{\mathrm{UO_2}} = 1$. The melting points and lattice parameters of MA-MOX and UO_2 used in Eq. (17) were the values obtained in the same ways mentioned in Eqs. (10) and (11).

In this study, *B*-values were tentatively evaluated by using the above Eqs. (16) and (17). The *B*-values evaluated by experiment and calculation are shown in Fig. 8. The experimental value of *B* was the average of *B*-values obtained from the experimental data of Np-MOX and Am-MOX. It is found from the calculation that the effects of Np- and Am-oxide additions on *B*-value are small, and that the *B*-value increases very slightly with increasing contents of Np- and Am-oxides. It is seen that the calculated *B*-values are a little smaller than the experimental value used in the derivation of *A*-values by best fittings, but *B*-values are nearly independent of the Np- and Am-oxide contents, as already described.

4. Conclusions

The thermal conductivities of MOX containing Np- and Am-oxides (Am-MOX and Np-MOX) were measured by the laser flash method in the temperature range from 900 to 1770 K. The obtained conductivities were normalized to those of 100% of the theoretical density by using the modified Maxwell–Eucken relationship [7]. The obtained results were analyzed together with the results on the Am-MOX obtained in by Morimoto et al. [7].

The thermal conductivities could be expressed in the temperature region below 1400 K by the simple equation, $\lambda = (A + BT)^{-1}$ derived from a classical phonon transport model. The values of A and B were evaluated by this equation. It was found that the A-values increased linearly with increasing Np-oxide and Am-oxide contents slightly, and the effect of Np-oxide content was smaller than that of Am-oxide content.

The reason for this was suggested to be the smaller extent of lattice distortions leading to phonon scattering in Np-MOX than in Am-MOX, because the difference of ionic radii between U and Np is smaller than that between U and Am.

The dependences of A-values on the Np- and Am-oxides were evaluated, assuming that B-value was constant and independent of Np- and Am-oxide contents, as similarly pointed out by previous studies [7,14]. The results were expressed as follows

$$\lambda_0 = (A + BT)^{-1}(\mathrm{W/m/K}),$$

$$A = 3.583 \times 10^{-1} \times z_1 + 6.317 \times 10^{-2} \times z_2 + 1.595 \times 10^{-2}(\mathrm{mK/W}),$$

$$B = 2.493 \times 10^{-4}(\mathrm{m/W}),$$

where z_1 and z_2 are the contents of Am- and Np-oxides, respectively. It was shown also in this result that the effect of MA addition content was smaller in Np-MOX than in Am-MOX.

The dependences of B-values on Np- and Am-oxide contents were tentatively evaluated by the Liebfried–Schlömann relationship for the intrinsic phonon resistivity. It was found that the obtained B-values was nearly independent of the Np- and Am-oxide contents and were a little smaller than the ones used in the derivation of A-values by best fittings.

Acknowledgements

The authors are pleased to acknowledge Mr. H. Uno, Mr. T. Tamura, Mr. H. Sugata, Mr. T. Sunaoshi and Mr. K. Shibata for their collaboration in the sample preparation, EPMA analyses and XRD. Special thanks are also given to Professor Emeritus of Kyushu University, Dr. H. Furuya for valuable discussions.

References

[1] K. Aizawa, Progr. Nucl. Energy 40 (2002) 349.
[2] M. Osaka, H. Serizawa, M. Kato, K. Nakajima, Y. Tachi, et al., J. Nucl. Sci. Technol. 44 (2007) 309.
[3] H.E. Schmidt, C. Sari, K. Richter, P. Gerontopoulos, J. Less Common Met. 121 (1986) 621.
[4] M. Katayama, J. Adachi, K. Kurosaki, M. Uno, S. Miwa, M. Osaka, K. Tanaka, S. Yamanaka, in: Mater. Res. Soc. Symp. Proc., vol. 1043E, Warrendale, PA, 2007, 1043-T09-06.
[5] T. Nishi, A. Itoh, M. Takano, M. Numata, M. Akabori, Y. Arai, K. Minato, J. Nucl. Mater. 376 (2008) 78.
[6] K. Kurosaki, M. Imamura, I. Sato, T. Namekawa, M. Uno, S. Yamanaka, J. Alloys Compd. 387 (2005) 9.
[7] K. Morimoto, M. Kato, M. Ogasawara, M. Kashimura, T. Abe, J. Nucl. Mater. 452 (2008) 54.
[8] M. Kato, H. Uno, T. Tamura, K. Morimoto, K. Konashi, Y. Kihara, in: Proceedings of the Eighth Actinide Conference, Actinides 2005, Manchester, UK, 2005, p. 367.
[9] T. Baba, A. Cezairliyan, Int. J. Thermophys. 15 (1994) 343.
[10] J.J. Carbajo, G.L. Yoder, S.G. Popov, V.K. Ivanov, J. Nucl. Mater. 299 (2001) 181.
[11] E.H.P. Cordfunke, R.J.M. Konings, Thermochemical Data for Reactor Materials and Fission Products, North-Holland, Amsterdam, 1990. p. 35.
[12] I. Barin, Thermochemical Data of Pure Substances, VCH Verlagsgesellschaft mbH, Weinheim, 1989.
[13] M. Hirai, J. Nucl. Mater. 173 (1990) 247.
[14] S. Fukushima, T. Ohmichi, A. Maeda, M. Handa, J. Nucl. Mater. 116 (1983) 287.
[15] V. Ambegaoker, Phys. Rev. 114 (1959) 488.
[16] P.G. Klemens, Proc. Phys. Soc. (London) A68 (1955) 1113.
[17] B. Abeles, Phys. Rev. 131 (1963) 1906.
[18] K. Richter, C. Sari, J. Nucl. Mater. 148 (1987) 266.
[19] M. Kato, K. Morimoto, H. Sugata, K. Konashi, M. Kashimura, T. Abe, J. Nucl. Mater. 373 (2008) 237.
[20] R.D. Shanon, Acta Crystallogr. A 32 (1976) 751.
[21] T. Ohmichi, S. Fukushima, A. Maeda, H. Watanabe, J. Nucl. Mater. 102 (1981) 40.
[22] R.L. Gibby, J. Nucl. Mater. 38 (1971) 163.
[23] C. Duriez, J.P. Alessandri, T. Gervais, Y. Philipponneau, J. Nucl. Mater. 277 (2000) 143.
[24] S. Ishimoto, M. Hirai, K. Ito, Y. Korei, J. Nucl. Sci. Technol. 31 (8) (1994) 796.
[25] M. Amaya, M. Hirai, T. Kubo, Y. Korei, J. Nucl. Mater. 231 (1996) 29.